Mixing of collinear plane wave pulses in elastic solids with quadratic nonlinearity

Zimu Chen
School of Materials Science and Engineering, Beihang University, Beijing, 100191, China

Guangxin Tang
Department of Mechanical Engineering, Northwestern University, Evanston, Illinois 60208

Youxun Zhao
School of Civil Engineering, Southwest Jiaotong University, Chengdu, China

Laurence J. Jacobs
School of Civil and Environmental Engineering, Georgia Institute of Technology, Atlanta, Georgia 30332-0355

Jianmin Qu[a)]
Department of Civil and Environmental Engineering, Northwestern University, Evanston, Illinois 60208

(Received 20 June 2014; revised 22 August 2014; accepted 16 September 2014)

This paper derives a set of necessary and sufficient conditions for generating resonant waves by two propagating time-harmonic plane waves. It is shown that in collinear mixing, a resonant wave can be generated either by a pair of longitudinal waves, in which case the resonant mixing wave is also a longitudinal wave, or by a pair of longitudinal and transverse waves, in which case the resonant wave is a transverse wave. In addition, the paper obtains closed-form analytical solutions to the resonant waves generated by two collinearly propagating sinusoidal pulses. The results show that amplitude of the resonant pulse is proportional to the mixing zone size, which is determined by the spatial lengths of the input pulses. Finally, numerical simulations based on the finite element method and experimental measurements using one-way mixing are conducted. It is shown that both numerical and experimental results agree well with the analytical solutions.
 [http://dx.doi.org/10.1121/1.4896567]

PACS number(s): 43.25.Dc, 43.25.Gf, 43.25.Zx, 43.25.Ba [ANN] Pages: 2389–2404

I. INTRODUCTION

Because of their ability to characterize damage in its early stages, nonlinear ultrasonic nondestructive evaluation (NDE) techniques have attracted a great deal of attention recently. Among the various nonlinear ultrasonic NDE techniques, the wave mixing method is relatively new, although the phenomenon of nonlinear wave mixing has been studied since the early 1960s.[1–4] Liu *et al*. develop a collinear wave mixing method to measure the acoustic nonlinearity parameter,[5] Tang *et al*. developed a scanning method based on collinear mixing to detect localized plastic deformation,[6] and Jiao *et al.*[7] used collinear wave mixing to detect micro-cracks. Non-collinear wave mixing methods were used by Demcenko *et al.*[8] to detect physical aging, by Croxford *et al.*[9] to study plasticity and fatigue, and by Escobar-Ruiz *et al.*[10] to characterize titanium diffusion bonds. Similar non-collinear wave mixing techniques were used by Demcenko *et al.*[11] to measure physical aging in thermoplastics and curing of epoxy.

These studies have demonstrated that nonlinear wave mixing techniques have some unique advantages over other nonlinear NDE techniques. For example, wave mixing methods allow the user to select the frequency to be monitored. This avoids unwanted harmonics that are typically generated by a number of electronic components in the measurement system. The wave mixing method enables the user to control the location where the waves are mixed, thus allowing localized measurements. More significant is the fact that such a controlled localized measurement enables scanning over a region of interest.

Of course, the wave mixing method is not without limitations. For one, although interactions occur between any two propagating waves, only when these two waves satisfy certain conditions is the generated mixing wave cumulative in that its amplitude grows with propagating distance within the region where these two wave mix. Such a growing mixing wave is called a resonant mixing wave, or a resonant wave. Experimentally, only these resonant waves can be detected with reasonable accuracy with the currently available ultrasonic measurement systems. Next, mixing of two waves generates a rather complex wave field, making it difficult to interpret the received signal. Therefore, to design effective NDE techniques based on wave mixing, the interactions between two nonlinear waves must be fully understood.

In their seminal work, Jones *et al.*[1] show that in order to generate a resonant wave (or a strong scattered wave as referred to in their paper), a necessary condition for the two primary waves is

$$\frac{\omega_1 \pm \omega_2}{\|\mathbf{k}_1 \pm \mathbf{k}_2\|} = c_L \text{ or } c_T, \tag{1}$$

[a)]Author to whom correspondence should be addressed. Electronic mail: j-qu@northwestern.edu

where ω_n and $\mathbf{k}_n$ ($n = 1, 2$) are the frequencies and the wave vectors of the two primary waves, and c_L and c_T are the phase velocity of the longitudinal and transverse waves, respectively. This necessary condition provides a useful guide for designing NDE techniques based on wave mixing.

However, as will be shown later in this paper, Eq. (1) is only a necessary condition for generating resonant waves. It is not sufficient. In this paper, we will first study the mixing of two propagating plane time-harmonic waves, and derive the necessary and sufficient conditions for generating resonant waves. We will then focus on collinear mixing, and solve the full wave field when two collinearly propagating sinusoidal pulses interact. The paper is arranged as follows. For completeness, Sec. II lists the relevant elastodynamics equations. Section III establishes the necessary and sufficient conditions for generating resonant waves by two propagating plane time-harmonic waves, while Sec. IV is devoted to the mixing of two collinearly propagating sinusoidal pulses. Exact solutions for the full wave field are obtained. In Sec. V, a finite element method is used to numerically simulate the interaction between two collinearly propagating sinusoidal pulses. The purpose of the numerical solution is to study the feasibility of using the finite element method to simulate mixing of nonlinear waves. Experimental measurements are conducted and reported in Sec. VI to demonstrate that the resonant waves are indeed measurable experimentally, and the measured results compare well with the predictions from the analytical solution. Finally, a summary and some conclusions are provided in Sec. VII.

II. WAVE MOTION IN ELASTIC SOLIDS WITH QUADRATIC NONLINEARITY

Consider a homogeneous solid. To describe the wave motion, we affix a Cartesian coordinate x_i ($i = 1, 2, 3$) to the solid, where the coordinate x_i is also used to label the material particle that was located at x_i in the initial (undeformed) configuration. This way of describing the wave motion is called the Lagrangian description and x_i is called the Lagrangian coordinate. At any given time t, the displacement of the particle x_i from its initial location is denoted by $u_i = u_i(\mathbf{x}, t)$.

The displacement equations of motion can be written as[12]

$$L_i[\mathbf{u}] \equiv \frac{1}{c_L^2}\frac{\partial^2 u_i}{\partial t^2} - \left(1 - \frac{1}{\kappa^2}\right)\frac{\partial^2 u_j}{\partial x_j \partial x_i} - \frac{1}{\kappa^2}\frac{\partial^2 u_i}{\partial x_j \partial x_j} = F_i[\mathbf{u}], \tag{2}$$

where $c_L = \sqrt{(\lambda + 2\mu)/\rho}$ and $c_T = \sqrt{\mu/\rho}$ are the longitudinal and transverse phase velocities, respectively, $\kappa = c_L/c_T$, λ and μ are the Lamé constants, and ρ is the mass density. On the right hand side, $F_i[\mathbf{u}]$ is a homogeneous quadratic function of the displacement vector $\mathbf{u} = [u_1, u_2, u_3]$.[12]

Asymptotically, by retaining terms up to the second order, the solution to Eq. (2) can be written as

$$u_i = u_i^{(0)} + u_i^{(1)}, \tag{3}$$

where $|u_i^{(0)}| \gg |u_i^{(1)}|$, and

$$L_i[\mathbf{u}^{(0)}] = 0, \qquad L_i[\mathbf{u}^{(1)}] = F_i[\mathbf{u}^{(0)}]. \tag{4}$$

In deriving the second equation of Eq. (4), we have used the fact that $F_i[\mathbf{u}^1] \ll F_i[\mathbf{u}^{(0)}]$.

If we consider waves that propagate in the x_1-direction in the form of

$$u_1 = u_1(x_1, t), \quad u_2 = u_2(x_1, t), \quad u_3 = 0, \tag{5}$$

only two of the equations of motion are non-trivial. Their right hand sides become

$$\begin{aligned} F_1[\mathbf{u}] &= \beta_L \frac{\partial u_1}{\partial x_1}\frac{\partial^2 u_1}{\partial x_1^2} + \frac{\beta_T}{\kappa^2}\frac{\partial u_2}{\partial x_1}\frac{\partial^2 u_2}{\partial x_1^2}, \\ F_2[\mathbf{u}] &= \frac{\beta_T}{\kappa^2}\left(\frac{\partial^2 u_1}{\partial x_1^2}\frac{\partial u_2}{\partial x_1} + \frac{\partial u_1}{\partial x_1}\frac{\partial^2 u_2}{\partial x_1^2}\right), \end{aligned} \tag{6}$$

where

$$\beta_L = 3 + \eta_L, \quad \beta_T = \kappa^2 + \eta_T \tag{7}$$

are called, respectively, the longitudinal and transverse acoustic nonlinearity parameters. In the above,

$$\eta_L = \frac{2(l + 2m)}{\lambda + 2\mu}, \qquad \eta_T = \frac{m}{\mu}, \tag{8}$$

where l, m, and n are the Murnaghan third order elastic constants. Clearly, η_L and η_T are related to the material nonlinearity.

III. MIXING OF TWO STEADY-STATE TIME HARMONIC WAVES

We consider the mixing of two primary plane waves in the x_1x_2-plane,

$$\begin{aligned} u_i^{(0)} &= U_1 d_i^{(1)} \cos(\omega_1 t - k_1 p_j^{(1)} x_j) \\ &\quad + U_2 d_i^{(2)} \cos(\omega_2 t - k_2 p_j^{(2)} x_j), \\ u_3^{(0)} &= 0, \end{aligned} \tag{9}$$

where $d_i^{(m)}$ and $p_i^{(m)}$ ($m = 1, 2$) are the displacement and propagation vectors, respectively, for the two primary waves. In this section, we implicitly assume that subscripts in the summation notation range from 1 to 2 only.

If the solid is linear elastic, it is well known that the two primary waves will simply propagate on their own without interacting with one another. However, in a nonlinear medium, not only each wave will generate its own higher harmonics, the two waves would also interact and generate an additional wave field.[1] In this section, we will focus on this additional wave field generated by the interactions between the two primary plane waves.

Substituting Eq. (9) into Eq. (6), and retaining only the cross terms between the two waves due to nonlinear interactions leads to

$$F_i[\mathbf{u}] = U_1 U_2 [b_i^+ \sin(\omega_+ t - k_j^+ x_j) + b_i^- \sin(\omega_- t - k_j^- x_j)], \tag{10}$$

where

$$\omega_{\pm} = \omega_1 \pm \omega_2, \quad k_j^{\pm} = k_1 p_j^{(1)} \pm k_2 p_j^{(2)}, \tag{11}$$

and $\mathbf{b}^{\pm} = (b_1^{\pm}, b_2^{\pm})^T$ are known functions of the materials and frequencies, which have been derived previously in Ref. 1. We note that Eq. (2) is a linear system of equations. Thus, its solution can be obtained by superimposing solutions corresponding to the different terms in Eq. (10).

It can be seen that a possible solution to the second equation of Eq. (4) might be written as

$$u_i^{(1)} = a_i^+ \sin(\omega_+ t - k_j^+ x_j) + a_i^- \sin(\omega_- t - k_j^- x_j), \tag{12}$$

where $\mathbf{a}^{\pm} = (a_1^{\pm}, a_2^{\pm})^T$ are constants to be determined. Substituting Eq. (12) into Eq. (2) yields a system of four algebraic equations for $\mathbf{a}^{\pm}$,

$$\mathbf{A}^{\pm}\mathbf{a}^{\pm} = U_1 U_2 \mathbf{b}^{\pm}, \tag{13}$$

where

$$\mathbf{A}^{\pm} = \begin{bmatrix} h_1^{\pm} & s^{\pm} \\ s^{\pm} & h_2^{\pm} \end{bmatrix}, \tag{14}$$

with

$$h_1^{\pm} = -\frac{1}{\kappa^2 c_L^2}\left\{\kappa^2 \omega_{\pm}^2 - c_L^2\left[\left(k_2^{\pm}\right)^2 + \kappa^2\left(k_1^{\pm}\right)^2\right]\right\}, \tag{15}$$

$$h_2^{\pm} = -\frac{1}{\kappa^2 c_L^2}\left\{\kappa^2 \omega_{\pm}^2 - c_L^2\left[\left(k_1^{\pm}\right)^2 + \kappa^2\left(k_2^{\pm}\right)^2\right]\right\}, \tag{16}$$

$$s^{\pm} = \frac{\kappa^2 - 1}{\kappa^2} k_1^{\pm} k_2^{\pm}. \tag{17}$$

The determinants of $\mathbf{A}^{\pm}$ are given by

$$D_{\pm} = \det(\mathbf{A}^{\pm}) = \frac{1}{\kappa^2}\left(k_j^{\pm}k_j^{\pm} - \frac{\omega_{\pm}^2}{c_L^2}\right)\left(k_j^{\pm}k_j^{\pm} - \frac{\omega_{\pm}^2}{c_T^2}\right). \tag{18}$$

If $D_+ D_- \neq 0$, Eq. (13) will have a unique solution given by

$$\mathbf{a}^{\pm} = U_1 U_2 (\mathbf{A}^{\pm})^{-1}\mathbf{b}^{\pm}. \tag{19}$$

Substituting Eq. (18) into Eq. (12) yields the solution to the wave fields generated by the nonlinear interactions between the two primary waves. It is seen that such waves propagate with constant amplitudes and frequencies that are the sum and difference of the frequencies of the two primary waves. In fact, even when $D_+ D_- = 0$, a unique solution to $\mathbf{a}^{\pm}$ may still exit if

$$\operatorname{rank}(\mathbf{A}^+|\mathbf{b}^+) = \operatorname{rank}(\mathbf{A}^+) \text{ or } \operatorname{rank}(\mathbf{A}^-|\mathbf{b}^-) = \operatorname{rank}(\mathbf{A}^-), \tag{20}$$

where $(\mathbf{A}^{\pm}|\mathbf{b}^{\pm})$ denotes the augmented matrix, i.e., a matrix obtained by appending the columns of $\mathbf{b}^{\pm}$ to $\mathbf{A}^{\pm}$.

For convenience, we call Eq. (12) with $\mathbf{a}^{\pm}$ being given by Eq. (19) the mixing wave field induced by the nonlinear interactions between the two primary waves. It is seen that such a mixing wave field generally consists of two propagating waves in the directions of $\mathbf{k}^+$ and $\mathbf{k}^-$, respectively.

A more interesting, and practically useful case is when $D_+ D_- = 0$, while either $\operatorname{rank}(\mathbf{A}^+|\mathbf{b}^+) \neq \operatorname{rank}(\mathbf{A}^+)$ or $\operatorname{rank}(\mathbf{A}^-|\mathbf{b}^-) \neq \operatorname{rank}(\mathbf{A}^-)$. In these cases, one or both of the sinusoidal functions in Eq. (12) become the eigenfunctions of the homogeneous equation of Eq. (4).

Thus, the solution to the second equation of Eq. (4) is no longer in the form of Eq. (12). In fact, the solution in these cases will grow linearly with the propagation distance. This phenomenon is called resonance. The waves generated by the nonlinear interaction under such resonant conditions will be called the resonant waves.

It follows from Eq. (18) that $D_+ D_- = 0$ is equivalent to

$$\left(k_j^{\pm}k_j^{\pm} - \frac{\omega_{\pm}^2}{c_L^2}\right)\left(k_j^{\pm}k_j^{\pm} - \frac{\omega_{\pm}^2}{c_T^2}\right) = 0. \tag{21}$$

Note that Eq. (21) is the resonant condition derived in Ref. 1. However, from the foregoing discussions, it is seen that $D_+ D_- = 0$ is only a necessary condition for generating resonant waves. The sufficient conditions are $D_+ D_- = 0$ and $\operatorname{rank}(\mathbf{A}^+|\mathbf{b}^+) \neq \operatorname{rank}(\mathbf{A}^+)$ or $\operatorname{rank}(\mathbf{A}^-|\mathbf{b}^-) \neq \operatorname{rank}(\mathbf{A}^-)$. In what follows, we will discuss several special cases to illustrate the application of such necessary and sufficient conditions.

A. Mixing of two collinear longitudinal plane waves

Without loss of generality, we consider the mixing of the following two collinear longitudinal waves,

$$\mathbf{p}_1 = \mathbf{p}_2 = \mathbf{d}_1 = \mathbf{d}_2 = (1, 0)^T. \tag{22}$$

Making use of Eq. (22) in Eqs. (10) and (14) leads to

$$\mathbf{b}^{\pm} = \mp \frac{\beta_L}{2c_L^3}\omega_1\omega_2 \begin{bmatrix} \omega_{\pm} \\ 0 \end{bmatrix},$$
$$\mathbf{A}^{\pm} = \begin{bmatrix} 0 & 0 \\ 0 & -\dfrac{(\kappa^2 - 1)\omega_{\pm}^2}{c_L^2 \kappa^2} \end{bmatrix}. \tag{23}$$

Obviously, $D_+ = D_- = 0$. Furthermore, one can show that $\operatorname{rank}(\mathbf{A}^{\pm}|\mathbf{b}^{\pm}) \neq \operatorname{rank}(\mathbf{A}^{\pm})$, which means that Eq. (12) is no longer a solution to Eq. (2). In other words, the mixing of two collinear longitudinal waves will generate a resonant wave. One can show by substitution that this resonant wave is a longitudinal wave given by

$$u_1^{(1)} = -\frac{\beta_L}{4c_L^2}\omega_1\omega_2 U_1 U_2 x_1 \left\{\cos\left[\omega_+\left(t - \frac{x_1}{c_L}\right)\right] - \cos\left[\omega_-\left(t - \frac{x_1}{c_L}\right)\right]\right\}, \quad u_2^{(1)} = 0. \tag{24}$$

We see that indeed the mixed wave grows with propagating distance x_1.

Interestingly, it can be shown that in the limit of $\omega_2 \to \omega_1 = \omega$ and $U_2 \to U_1 = U$, Eq. (24) reduces to

$$u_1^{(1)} = \frac{\beta_L}{4c_L^2}\omega^2 U^2 x_1 \left\{1 - \cos\left[2\omega\left(t - \frac{x_1}{c_L}\right)\right]\right\}. \tag{25}$$

This is the same as the well-known generation of second harmonic. In fact, by including the terms generated by U_1^2 and U_2^2 in $F_i[\mathbf{u}]$, the total solution now becomes

$$u_1^{(1)} = 2U\sin\left[\omega\left(t - \frac{x_1}{c_L}\right)\right] + \frac{\beta_L U^2 k_L^2 x_1}{2}\left\{1 - \cos\left[2\omega\left(t - \frac{x_1}{c_L}\right)\right]\right\}. \tag{26}$$

This is the well-known solution to a propagating longitudinal wave in an elastic solid with quadratic nonlinearity, if the amplitude of the primary wave is $2U$. In other words, the generation of second harmonic by a longitudinal wave is really the result of "self-mixing" of the longitudinal wave with itself.

B. Mixing of two collinear transverse plane waves

Again, without loss of generality, we consider the mixing of the following two collinear transverse waves,

$$\mathbf{p}_1 = \mathbf{p}_2 = (1, 0)^T, \quad \mathbf{d}_1 = \mathbf{d}_2 = (0, 1)^T. \tag{27}$$

It is easy to show that

$$\mathbf{A}^{\pm} = \begin{bmatrix} \dfrac{(\kappa^2 - 1)\omega_{\pm}^2}{c_L^2} & 0 \\ 0 & 0 \end{bmatrix}, \quad \mathbf{b}^{\pm} = \mp \frac{\beta_T}{2\kappa^2 c_T^3}\omega_1\omega_2 \begin{bmatrix} \omega_{\pm} \\ 0 \end{bmatrix}. \tag{28}$$

Clearly, $D_+ = D_- = 0$. However, we also have $\mathrm{rank}(\mathbf{A}^{\pm}|\mathbf{b}^{\pm}) = \mathrm{rank}(\mathbf{A}^{\pm}) = 1$. Thus, there is still a unique solution to Eq. (13), which is given by

$$u_1^{(1)} = \frac{\beta_T \omega_1 \omega_2 U_1 U_2}{2c_T(\kappa^2 - 1)}\left\{\frac{1}{\omega_-}\sin\left[\omega_-\left(t - \frac{x_1}{c_T}\right)\right] - \frac{1}{\omega_+}\sin\left[\omega_+\left(t - \frac{x_1}{c_T}\right)\right]\right\}, \quad u_2^{(1)} = 0. \tag{29}$$

We see that the mixing wave generated by two collinear transverse shear waves consists of two longitudinal waves of constant amplitude with frequencies ω_- and ω_+, respectively. However, they are not resonant waves, i.e., they do not accumulate in amplitude as they propagate through the mixing zone. Another interesting phenomenon is that the velocity of these mixing longitudinal waves is c_T instead of c_L. This is possible only as mixing waves accompanied by the two primary transverse waves. Such a mixing wave cannot propagate outside the mixing zone.

C. Mixing of a collinear longitudinal and a transverse plane waves

Let us first consider the case when the two waves propagate in the same direction, i.e.,

$$\mathbf{p}_1 = \mathbf{p}_2 = (1, 0)^T, \ \mathbf{d}_1 = (0, 1)^T, \ \mathbf{d}_2 = \mathbf{p}_2. \tag{30}$$

Consequently,

$$\begin{aligned} \mathbf{A}^{\pm} &= -\frac{\kappa - 1}{c_T^2\kappa^4}\begin{bmatrix} -\kappa^2\omega_1(\omega_1 + \kappa\omega_1 \pm 2\omega_2) & 0 \\ 0 & \omega_2(\omega_2 + \kappa\omega_2 \pm 2\kappa\omega_1) \end{bmatrix}, \\ \mathbf{b}^{\pm} &= -\frac{\beta_T \omega_1 \omega_2}{2c_T^3\kappa^4}\begin{bmatrix} 0 \\ \omega_2 \pm \kappa\omega_1 \end{bmatrix}. \end{aligned} \tag{31}$$

It can be shown that $D_+D_- = 0$ has two physically meaningful roots, $\omega_2/\omega_1 = 2\kappa/(\kappa + 1)$ and $\omega_2/\omega_1 = (\kappa + 1)/2$. However, only the former leads to $\mathrm{rank}(\mathbf{A}^-|\mathbf{b}^-) \neq \mathrm{rank}(\mathbf{A}^-)$. That is, only when $\omega_2/\omega_1 = 2\kappa/(\kappa + 1)$, a resonant wave occurs, which is given by

$$
\begin{aligned}
u_1^{(1)} &= 0,\\
u_2^{(1)} &= M_1 x_1 \cos\left[\omega_-\left(t+\frac{x_1}{c_T}\right)\right]\\
&\quad -\frac{\beta_T \omega_1 U_1 U_2}{8c_T(\kappa^2-1)}(\kappa+3)\sin\left[\omega_+\left(t-\frac{x_1}{c_+}\right)\right],
\end{aligned}
\tag{32}
$$

where

$$
M_1 = \frac{\beta_T \omega_1^2 U_1 U_2}{2c_T^2(\kappa+1)}, \quad c_+ = \frac{k_+}{\omega_+} = \frac{3\kappa+1}{\kappa+3}c_T. \tag{33}
$$

Clearly, the first term on the right hand side of Eq. (32) represents a resonant transverse wave propagating in the opposite direction as that of the two primary waves. Its phase velocity is the transverse wave phase velocity, and its frequency is $\omega_- = \omega_1 - \omega_2$.

Next, consider the case when the two waves propagate in the opposite directions, e.g.,

$$
\mathbf{p}_1 = -\mathbf{p}_2 = (1,0)^T, \quad \mathbf{d}_1 = (0,1)^T, \quad \mathbf{d}_2 = \mathbf{p}_2. \tag{34}
$$

This leads to

$$
\mathbf{A}^{\pm} = -\frac{\kappa+1}{c_T^2\kappa^4}\begin{bmatrix} \kappa^2\omega_1(\omega_1-\kappa\omega_1\pm 2\omega_2) & 0 \\ 0 & \omega_2(-\omega_2+\kappa\omega_2\pm 2\kappa\omega_1)\end{bmatrix}, \tag{35}
$$

$$
\mathbf{b}^{\pm} = \frac{\beta_T\omega_1\omega_2}{2c_T^3\kappa^4}\begin{bmatrix} 0 \\ \omega_2 \mp \kappa\omega_1 \end{bmatrix}. \tag{36}
$$

It can be shown that $D_+D_- = 0$ has two physically meaningful roots, $\omega_2/\omega_1 = 2\kappa/(\kappa-1)$ and $\omega_2/\omega_1 = (\kappa-1)/2$. Only the former leads to $\mathrm{rank}(\mathbf{A}^-|\mathbf{b}^-) \neq \mathrm{rank}(\mathbf{A}^-)$. That is, only when $\omega_2/\omega_1 = 2\kappa/(\kappa-1)$, does a resonant wave occur, which is given by

$$
\begin{aligned}
u_1^{(1)} &= 0,\\
u_2^{(1)} &= -M_2 x_1 \cos\left[\omega_-\left(t+\frac{x_1}{c_T}\right)\right]\\
&\quad +\frac{\beta_T \omega_1 U_1 U_2}{8c_T(\kappa^2-1)}(\kappa-3)\sin\left[\omega_+\left(t-\frac{x_1}{c_-}\right)\right],
\end{aligned}
\tag{37}
$$

where

$$
M_2 = \frac{\beta_T \omega_1^2 U_1 U_2}{2c_T^2(\kappa-1)}, \quad c_- = \frac{k_-}{\omega_-} = \frac{3\kappa-1}{\kappa-3}c_T. \tag{38}
$$

Again, the first term on the right hand side of Eq. (37) represents a resonant transverse wave propagating in the direction opposite to that of the primary transverse wave.

IV. COLLINEAR MIXING OF TIME HARMONIC LONGITUDINAL AND TRANSVERSE PULSES

In this section, we investigate the collinear mixing of a time-harmonic longitudinal pulse and a time-harmonic transverse pulse, both are propagating along the x_1-direction. For brevity, we will drop the subscript in our notation by adopting $x = x_1$, $u = u_1^{(1)}$, $v = u_2^{(1)}$, $V = U_1$ and $U = U_2$. Further, for clarity, we let $\omega_1 = \omega_T$, $\omega_2 = \omega_L$, where ω_T and ω_L are the circular frequencies of the longitudinal and transverse waves, respectively. When both pulses are emitted at $x = 0$ and propagate in the positive x-direction, it is called one-way mixing. When the transverse pulse is emitted at $x = 0$ and propagates in the positive x-direction, while the longitudinal pulse is emitted at $x = L$ and propagates in the negative x-direction, it is called two-way mixing. We will study these two cases separately.

A. One-way mixing

The primary waves fields can be written as

$$
u_1^{(0)} = U\cos\left[\omega_L\left(t-t_L-\frac{x}{c_L}\right)\right]P\left(t-t_L-\frac{x}{c_L},\tau_L\right), \tag{39}
$$

$$
u_2^{(0)} = V\cos\left[\omega_T\left(t-t_T-\frac{x}{c_T}\right)\right]P\left(t-t_T-\frac{x}{c_T},\tau_T\right), \tag{40}
$$

where t_L and t_T are the triggering times when the longitudinal and transverse pulses are generated, respectively. The function $P(t,\tau)$ in Eq. (40) defines a rectangular pulse

$$
P(t,\tau) = \mathrm{H}(t)\mathrm{H}(\tau - t), \tag{41}
$$

where $\mathrm{H}(t)$ is the Heaviside step function, and $\tau_{L,T} = 2n_{L,T}\pi/\omega_{L,T}$ with $n_{L,T}$ being positive integers. Clearly, $\tau_{L,T}$ defines the temporal length of the pulses. For definitiveness and without loss of generality, we assume that

$$
t_T + \tau_T < t_L, \quad c_L\tau_L < c_T\tau_T. \tag{42}
$$

The first of the above means that the longitudinal pulse is not generated until the transverse pulse has completely left $x = 0$, and the second indicates that the spatial length of the transverse pulse is longer than that of the longitudinal pulse.

Substituting Eqs. (39)–(40) into Eq. (10) yields $F_1[\mathbf{u}^{(0)}] = 0$ and

$$
\begin{aligned}
F_2[\mathbf{u}^{(0)}] &= [B_+\sin(\omega_+ t - k_+ x - \phi_+)\\
&\quad + B_-\sin(\omega_- t - k_- x - \phi_-)]Q(x,t),
\end{aligned}
\tag{43}
$$

where

$$B_{\pm} = \frac{UV\beta_T\omega_L\omega_T}{2\kappa^2 c_L c_T}k_{\pm}, \quad \omega_{\pm} = \omega_T \pm \omega_L,$$
$$k_{\pm} = k_T \pm k_L, \quad \phi_{\pm} = t_T\omega_T \pm t_L\omega_L, \tag{44}$$

$$Q(x,t) = P\left(t - t_L - \frac{x}{c_L}, \tau_L\right) P\left(t - t_T - \frac{x}{c_T}, \tau_T\right). \tag{45}$$

It follows from the previous section that a resonant wave occurs when $\omega_L = 2\kappa\omega_T/(\kappa+1)$ and the resonant frequency and the corresponding wavenumber are, respectively,

$$\omega_R = -\omega_- = \omega_L - \omega_T = \frac{c_L - c_T}{c_L + c_T}\omega_T,$$
$$k_- = k_T - k_L = \frac{\omega_R}{c_T}. \tag{46}$$

Thus, the resonant wave can only be generated by the second term on the right hand side of Eq. (43). Thus, by introducing

$$f(x,t) = c_L^2 B_- \sin\left[\omega_R\left(t + \frac{x}{c_T}\right) + \phi_-\right] Q(x,t) \tag{47}$$

the governing equation for the resonant wave follows directly from Eq. (6),

$$\frac{\partial^2 v(x,t)}{\partial t^2} - c_T^2 \frac{\partial^2 v(x,t)}{\partial x^2} = f(x,t). \tag{48}$$

The corresponding Green's function problem is given by

$$\frac{\partial^2 v(x,t)}{\partial t^2} - c_T^2 \frac{\partial^2 v(x,t)}{\partial x^2} = \delta(t-\tau)\delta(x-s). \tag{49}$$

The solution is well-known,

$$G(x-s, t-\tau) = \frac{1}{2c_T}\mathrm{H}\left(t - \tau - \frac{|x-s|}{c_T}\right). \tag{50}$$

Thus, the solution to Eq. (48) can be written as

$$v(x,t) = \frac{1}{2c_T}\int_{-\infty}^{\infty}\int_{-\infty}^{\infty} f(s,\tau)\mathrm{H}\left(t - \tau - \frac{|x-s|}{c_T}\right) d\tau ds. \tag{51}$$

Making use of Eq. (47) in Eq. (51) yields

$$v(x,t) = -\frac{c_L^2 B_-}{2c_T}\int_{-\infty}^{\infty}\int_{-\infty}^{\infty} \sin\left[\omega_R\left(\tau + \frac{s}{c_T}\right) + \phi_-\right] \times Q(s,\tau)\mathrm{H}\left(t - \tau - \frac{|x-s|}{c_T}\right) ds d\tau. \tag{52}$$

We are interested in the signals received at $x = 0$, i.e.,

$$v(0,t) = -\frac{c_L^2 B_-}{2c_T}\int_{-\infty}^{\infty}\int_{-\infty}^{\infty} \sin\left[\omega_R\left(\tau + \frac{s}{c_T}\right) + \phi_-\right] \times Q(s,\tau)\mathrm{H}\left(t - \tau - \frac{|s|}{c_T}\right) ds d\tau. \tag{53}$$

The integral is carried out in Appendix A,

$$v(0,t) = M_1\left(\frac{c_L\tau_L}{\kappa+1}\right) g(t, n_L, \phi_-) \tag{54}$$

where M_1 is given by the first of Eq. (33),

$$g(t,n_L,\phi_-) = \begin{cases} \dfrac{t-t_1}{t_2-t_1}\cos(\omega_R t + \phi_-) - \dfrac{1}{2n_L\pi}[\sin(\omega_R t + \phi_-) - \sin(\omega_R t_1 + \phi_-)] & \text{for } t_1 < t < t_2 \\ \cos(\omega_R t + \phi_-) & \text{for } t_2 < t < t_3 \\ \dfrac{t_4-t}{t_4-t_3}\cos(\omega_R t + \phi_-) - \dfrac{1}{2n_L\pi}[\sin(\omega_R t_4 + \phi_-) - \sin(\omega_R t + \phi_-)] & \text{for } t_3 < t < t_4, \end{cases} \tag{55}$$

where n_L is the number of cycles in the longitudinal pulse, and t_1, t_2, t_3, and t_4 are given in Appendix A. In deriving Eqs. (54) and (55), we have used the fact that

$$t_2 - t_1 = t_4 - t_3 = \frac{2c_L\tau_L}{c_L - c_T}. \tag{56}$$

Several observations can be made about Eq. (54). First, the amplitude of $v(0, t)$ is proportional to M_1, which is the same factor that also appears in Eq. (32) for the one-way mixing of a longitudinal wave and a transverse wave of infinite extent.

Second, as in the case of Eq. (32), where the amplitude of $v(0, t)$ grows with the propagation distance of the resonant wave, the amplitude of $v(0, t)$ given in Eq. (54) is proportional to $c_L\tau_L/(\kappa+1)$. This result is derived for $c_L\tau_L < c_T\tau_T$, see Eq. (42). It is shown in Appendix A that for $c_T\tau_T < c_L\tau_L < c_T\tau_T\ (\kappa+1)/2$, the results are the same, while for $c_L\tau_L > c_T\tau_T\ (\kappa+1)/2$, the amplitude of $v(0, t)$ will be proportional to $c_T\tau_T/2$. In other words, the amplitude of $v(0, t)$ is proportional to $l_m = \min\{c_L\tau_L/(\kappa+1),\ c_T\tau_T/2\}$. This can be explained by how the resonant wave is generated. To resonate, two conditions must be met, namely, (i) there needs to be a region of finite length over which both longitudinal and

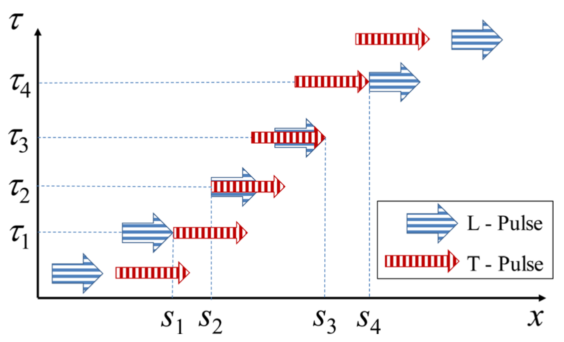

FIG. 1. (Color online) Schematic of the time τ_i and location s_i when the mixing signal occurs. The mixing signal occurs at time τ_i and location s_i will arrive the receiver at $x=0$ at $t_i = \tau_i + s_i/c_T$.

transverse waves co-exist, and (ii) over this region, the mixing wave is generated coherently (in phase). We will call this finite region the mixing zone, and the amplitude of the resonant wave is proportional to the mixing zone size according to Sec. III. It is easy to see that (ii) is met when $\omega_L = 2\kappa\omega_T/(\kappa+1)$ for one-way mixing and when $\omega_L = 2\kappa\omega_T/(\kappa-1)$ for two-way mixing. To identify the mixing zone, however, is not straightforward. Let us first look at the case of $c_L\tau_L < c_T\tau_T$ as illustrated in Fig. 1. The mixing signal begins to appear at $t=\tau_1$ when the front of the longitudinal pulse catches the rear of the transverse pulse. After the longitudinal pulse enters into the transverse pulse, an overlap region is created. This overlap region increases linearly with time until the entire longitudinal pulse is completely inside the transverse pulses at $t=\tau_2$, i.e., when the rear of the longitudinal pulse is located at $x=s_2$, see Fig. 1. Clearly, the maximum overlap region is $c_L\tau_L$, the spatial length of the longitudinal pulse. However, this overlap region is not the mixing zone. This can be seen, for example, by considering the mixing signal generated by the front of the longitudinal pulse at the location $x = s_2 + c_L\tau_L$ and time τ_2. Once generated, this particular mixing signal will propagate backward toward the rear of the longitudinal pulse. The mixing zone is then measured from $x = s_2 + c_L\tau_L$ (where the mixing signal is generated at time τ_2) to the rear of the longitudinal pulse. However, as this particular mixing signal propagates toward the rear of the longitudinal pulse, the rear of the longitudinal wave also propagates toward the incoming mixing signal. So, by the time that this particular mixing signal encounters the rear of the longitudinal pulse, the rear of the longitudinal pulse is no longer at $x=s_2$. It has advanced to a new location $x = s_2 + \Delta x$. Therefore, the maximum mixing zone over which the mixing signal accumulates is $l_m = c_L\tau_L - \Delta x$. It is easy to see that Δx must satisfy $\Delta x/c_L = (c_L\tau_L - \Delta x)/c_T$, which means that $l_m = c_L\tau_L/(\kappa+1)$. Similarly, one can show that this is also the maximum mixing zone size even when $c_T\tau_T < c_L\tau_L < c_T\tau_T(\kappa+1)/2$.

If $c_L\tau_L > c_T\tau_T\ (\kappa+1)/2$, the longitudinal pulse is spatially long enough so that the mixing signal generated by the front of the longitudinal pulse will first encounter the rear of the transverse pulse. Thus, the mixing zone is measured from where the signal is generated to the rear of the transverse pulse which also moves forward with velocity c_T. Following the discussions in the previous paragraph, the maximum mixing zone size in this case is $l_m = c_T\tau_T/2$.

Third, it is easy to see that $|g(t,n_L)| \le 2$. In fact, if the longitudinal wave has 10 or more cycles, $1/(2n_L\pi) \le 1.6\%$. Thus, the terms containing the sine function become negligible so that $|g(t,n_L)| \approx 1$. Finally, $|g(t,n_L)|$ is zero until $t=t_1$. It then increases linearly to $|g(t,n_L)|=1$ until $t=t_2$. Between $t_2<t<t_3$, it remains unchanged $|g(t,n_L)|=1$. After t_3, $|g(t,n_L)|$ decreases linearly and becomes zero at $t=t_4$. This means that the envelope of the waveform is a hexagon, see, e.g., Fig. 3 and Fig. 6. When $c_L\tau_L = c_T\tau_T\ (\kappa+1)/2$, one has $t_2=t_3$. Thus the hexagon becomes a rhombus (diamond).

The physical meaning of t_1, t_2, t_3, and t_4 is rather clear. Because of Eq. (42), the longitudinal pulse is spatially shorter than the transverse pulse. The transverse pulse is generated first at $t=t_T$. At $t=t_L$, the longitudinal wave is generated. By then, the rear of the transverse pulse has already left $x=0$. Later, the longitudinal pulse catches the transverse pulse. First, at $t=\tau_1$, the front of the longitudinal pulse comes into contact with the rear of the transverse pulse, see Fig. 1. Clearly, τ_1 must satisfy $(\tau_1 - t_L)c_L = (\tau_1 - t_T - \tau_T)c_T$. The spatial location when this happens is at $x = s_1 = (\tau_1 - t_L)c_L$. From this time on, the two pulses start mixing. The mixing generates a resonant transverse wave that propagates toward $x=0$. The time that the resonant transverse wave first arrives at $x=0$ is thus $t_1 = \tau_1 + s_1/c_T$. As time progresses, the longitudinal pulse invades the transverse pulse, and eventually enters into the transverse pulse completely, i.e., when the rear of the longitudinal pulse coincides with the rear of the transverse pulse. If this happens at $t=\tau_2$, then τ_2 must satisfy $(\tau_2 - t_L - \tau_L)c_L = (\tau_2 - t_T - \tau_T)c_T$, and the corresponding location is $x = s_2 = (\tau_2 - t_L - \tau_L)c_L$. The time it takes for the resonant signal generated at this moment to arrive at $x=0$ is thus $t_2 = \tau_2 + s_2/c_T$. Later, the front of the longitudinal pulse begins to exit the transverse pulse at $t=\tau_3$ and $x = s_3 = (\tau_3 - t_L)c_L$, where τ_3 is determined from $(\tau_3 - t_L)c_L = (\tau_3 - t_T)c_T$. The resonant signal generated at moment the $t=\tau_3$ and the location $x=s_3$ will arrive at $x=0$ at time $t_3 = \tau_3 + s_3/c_T$. Finally, the entire longitudinal pulse passes through the transverse pulse so that at $t=\tau_4$ the rear of the longitudinal wave begins to leave the front of the transverse pulse at $x = s_4 = (\tau_4 - t_L - \tau_L)c_L$, where τ_4 should satisfy $(\tau_4 - t_L - \tau_L)c_L = (\tau_4 - t_T)c_T$. The signal of the resonant wave generated by the rear of the longitudinal pulse and the front of the transverse pulse at the moment of the separation arrives at $x=0$ at time $t_4 = \tau_4 + s_4/c_T$.

B. Two-way mixing

Let a transverse pulse start at $x=0$ toward the positive x-direction, and a longitudinal pulse start at $x=L$ toward the negative x-direction, i.e., the primary waves fields are given by

$$u_1^{(0)} = U\cos\left[\omega_L\left(t - t_L - \frac{L-x}{c_L}\right)\right]P\left(t - t_L - \frac{L-x}{c_L}, \tau_L\right), \tag{57}$$

$$u_2^{(0)} = V\cos\left[\omega_T\left(t - t_T - \frac{x}{c_T}\right)\right]P\left(t - t_T - \frac{x}{c_T}, \tau_T\right). \tag{58}$$

Obviously, we need to assume that $c_T\tau_T + c_L\tau_L < L$ so there is enough room between $x = 0$ and $x = L$ for the two pulses to mix.

In the derivation below, we will, without losing generality, consider the case when $c_T\tau_T(\kappa - 1)/2 < c_L\tau_L < c_T\tau_T$, where we have implicitly assumed that $c_L < 3c_T$ which is the case for most engineering materials of interest. Substituting Eqs. (57) and (58) into Eq. (10) yields $F_1[\mathbf{u}^{(0)}] = 0$,

$$\begin{aligned} F_2[\mathbf{u}^{(0)}] = [&B_+ \sin(\omega_- t - k_+ x - \phi_-) \\ &- B_- \sin(\omega_+ t - k_- x - \phi_+)]Q(x,t), \end{aligned} \tag{59}$$

where $B_\pm$, $\omega_\pm$, $k_\pm$, and $\phi_\pm$ are all the same as defined previously. However,

$$Q(x,t) = P\left(t - t_L - \frac{L - x}{c_L}, \tau_L\right)P\left(t - t_T - \frac{x}{c_T}, \tau_T\right). \tag{60}$$

As shown in Sec. III, for two-way mixing, a resonant wave occurs when $\omega_L/\omega_T = 2\kappa/(\kappa - 1)$ and the resonant frequency and the corresponding wavenumber are, respectively,

$$\begin{aligned} \omega_R &= -\omega_- = \omega_L - \omega_T = \frac{c_L + c_T}{c_L - c_T}\omega_T, \\ k_+ &= k_T + k_L = \frac{\omega_R}{c_T}. \end{aligned} \tag{61}$$

Thus, the resonant wave can only be generated by the first term on the right hand side of Eq. (59). Following the solution procedure for the one-way mixing case, we can write the signal received at $x = 0$ as

$$\begin{aligned} v(0,t) = &-\frac{c_L^2 B_+}{2c_T}\int_{-\infty}^{\infty}\int_{-\infty}^{\infty} \sin\left[\omega_R\left(\tau + \frac{s}{c_T}\right) - \phi_-\right] \\ &\times Q(s,\tau)\mathrm{H}\left(t - \tau - \frac{|s|}{c_T}\right)ds d\tau. \end{aligned} \tag{62}$$

The integral is carried out in Appendix B

$$v(0,t) = M_2\left(\frac{c_T\tau_T}{2}\right)g(t, n_T, -\phi_-), \tag{63}$$

where M_2 is given by the first of Eq. (38), and the expression of $g(t, n_T, -\phi_-)$ is given in Eq. (55) with the understanding that the t_1, t_2, t_3, and t_4 in $g(t, n_T, -\phi_-)$ are replaced by those given in Appendix B. In deriving Eq. (63), we have used the fact that

$$t_2 - t_1 = t_4 - t_3 = \frac{\kappa - 1}{\kappa + 1}\tau_T. \tag{64}$$

In this case, t_1 is the arrival time of the mixing signal between the front of the longitudinal pulse and the rear of the transverse pulse, t_2 is the arrival time of the mixing signal between the front of the longitudinal pulse and the front of the transverse pulse, t_3 is the arrival time of the mixing signal between the rear of the longitudinal pulse and the rear of the transverse pulse, and t_4 is the arrival time of the mixing signal between the rear of the longitudinal pulse and the front of the transverse pulse.

Note that the first mixing signal is generated at time $t = \tau_1$ when the fronts of both pulses meet. However, this signal does not arrive at $x = 0$ until t_2, while the first signal arrived at $x = 0$ is generated by the front of the front of the longitudinal pulse and the rear of the transverse pulse when they meet at $t = \tau_3 > \tau_1$. In other words, the mixing signal generated first is not the first to arrive at $x = 0$. Instead, the mixing signal generated later by the front of the longitudinal pulse and the rear of the transverse pulse arrives at $x = 0$ first, because its location of mixing is closer to $x = 0$. This is different from the one-way mixing case where the first generated mixing signal arrives first.

Equation (63) says that the amplitude of $v(0, t)$ for two-way mixing is proportional to M_2, which is the same factor that appears in Eq. (37) for the two-way mixing of a longitudinal wave and a transverse wave of infinite extent. In addition, the amplitude of $v(0,t)$ is also proportional to $c_T\tau_T/2$ for the case of $c_T\tau_T$ $(\kappa - 1)/2 < c_L\tau_L < c_T\tau_T$ as derived above. It is shown in Appendix B that the results are the same for $c_L\tau_L > c_T\tau_T$, while for $c_L\tau_L < c_T\tau_T$ $(\kappa - 1)/2$, the amplitude of $v(0, t)$ is proportional to $c_L\tau_L/(\kappa - 1)$. In other words, the amplitude of $v(0,t)$ is proportional to $l_m = \min\{c_T\tau_T/2,\ c_L\tau_L/(\kappa - 1)\}$. Again, this can be explained by how the resonant wave is generated. For example, the first mixing signal begins to appear at $t = \tau_1$ when the two opposite-propagating pulses come into contact at $x = s_3$, see Fig. 2. This particular mixing signal will propagate toward the rear of the transverse pulse, along with the longitudinal pulse. Since the longitudinal pulse is faster, its front immediately bypasses the mixing signal it generated. Therefore, this particular mixing signal will propagate inside a zone where both longitudinal and transverse waves co-exist, until it either encounters the rear of the transverse pulse [when $c_L\tau_L > c_T\tau_T$ $(\kappa - 1)/2$], or is left behind by the rear of the longitudinal pulse [when $c_L\tau_L < c_T\tau_T$ $(\kappa - 1)/2$]. In the former, the maximum mixing zone l_m satisfies $l_m/c_T = (c_T\tau_T - l_m)/c_T$, which yields $l_m = c_T\tau_T/2$, and in the latter, the maximum mixing zone size satisfies $l_m/c_T = (c_L\tau_L + l_m)/c_L$, which yields $l_m = c_L\tau_L/(\kappa - 1)$.

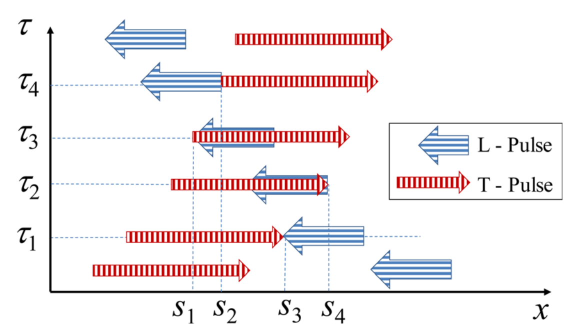

FIG. 2. (Color online) Schematic of the time τ_i and location s_i when the mixing signal occurs.

TABLE. I. Material properties used in the numerical simulation.

ρ (kg/m^3)	λ (MPa)	μ (MPa)	m (MPa)	n (MPa)	l (MPa)
2.7×10^3	5.11×10^4	2.63×10^4	-3.20×10^5	-2.82×10^5	-1.26×10^5

V. NUMERICAL SIMULATIONS BY THE FINITE ELEMENT METHOD

The analytical solutions derived in Sec. IV are for plane waves in semi-infinite domains. In reality, ultrasonic tests are usually conducted on finite size samples, and the pulses are generated by transducers of finite aperture as well. Thus, the analytical solutions derived above may not be sufficient to interpret actual testing results due to the divergence of the wave beam and the reflections from the sample boundaries. In order to accurately interpret the experimental data, it is necessary to simulate the actual wave fields generated by finite-size transducers in finite-size samples. In this section, we investigate the feasibility of using the finite element method (FEM) to simulate nonlinear wave mixing. To this end, plane wave pulses are simulated and the results are compared with the analytical results in Sec. IV. The purpose is to determine the mesh size in the FEM simulation for capturing the resonant waves.

The FEM simulations are conducted using the commercial software ABAQUS. Finite strain deformation and hyperelastisty constitutive laws with quadratic nonlinearity are used. The material properties used in the simulation are listed in Table I. These properties are approximately those of polycrystalline aluminum (AL7075).[13] From Table I, the corresponding phase velocities are $c_L = 6198$ m/s and $c_T = 3122$ m/s.

To simulate plane waves, a rectangular strip of $100\,\text{mm} \times 5\,\text{mm}$ is used in our FEM model. The model consists of $\sim$800 000 four-node plane strain (CPE4R) elements. A plane wave longitudinal pulse and a plane wave transverse pulse are generated from either the same end (one-way mixing) or opposite ends (two-way mixing) of the sample. The source to generate the pulses is uniformly distributed over the entire end surfaces of the rectangular strip, and periodic boundary conditions are used on the top and bottom surfaces of the rectangular strip.

The transverse pulse contains 10 cycles and the longitudinal pulse contain five cycles. The amplitude used is $V = 1 \times 10^{-4}$ mm for the transverse wave, and $U = 1 \times 10^{-5}$ mm for the longitudinal wave.

For one-way mixing, the frequencies used are $\omega_T = 7.5$ MHz for the transverse wave and $\omega_L = 10$ MHz for the longitudinal wave, which satisfy the resonant condition $\omega_L/\omega_T = 2\kappa/(\kappa+1)$. The corresponding resonant frequency is $\omega_R = 2.5$ MHz. For two-way mixing, the frequencies used are $\omega_T = 2.5$ MHz and $\omega_L = 10$ MHz for the longitudinal wave, which satisfy the resonant condition $\omega_L/\omega_T = 2\kappa/(\kappa-1)$. The corresponding resonant frequency is $\omega_R = 7.5$ MHz. In both cases, it is estimated that the shortest wavelength is about 20 times of the largest element size. This is consistent with the general rule of thumb[14,15] for FEM simulations of wave motion in elastic solids.

Shown in Figs. 3(b) and 4(b) are the FEM results of the frequency spectra of the resonant waves generated by one-way and two-way mixing, respectively. The corresponding time-domain waveforms are shown in Figs. 3(a) and 4(a) with the dashed lines. The superimposed solid lines are the corresponding waveforms computed from the analytical solution derived in the previous section. The excellent comparison shows that our FEM simulations are capable of capturing accurately the mixing waves. Further, using an element size that is about 5% of the shortest wavelength seems to provide sufficient accuracy when compared with analytical solutions.

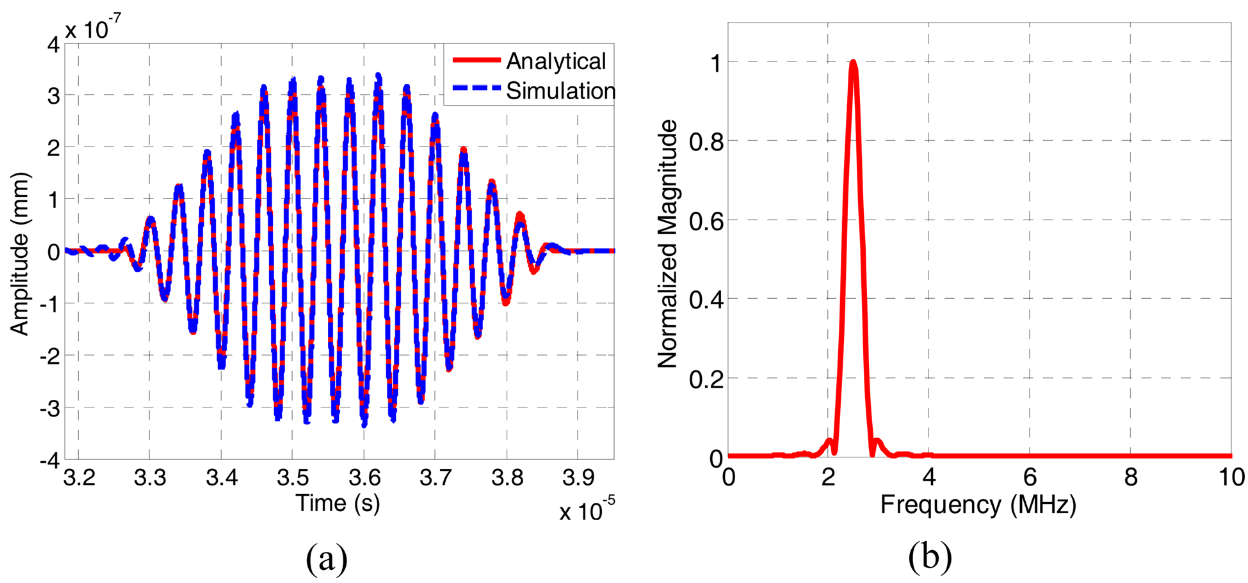

FIG. 3. (Color online) Waveform (a) and frequency spectrum (b) of the resonant wave generated by the one-way mixing of a longitudinal and a transverse pulse.

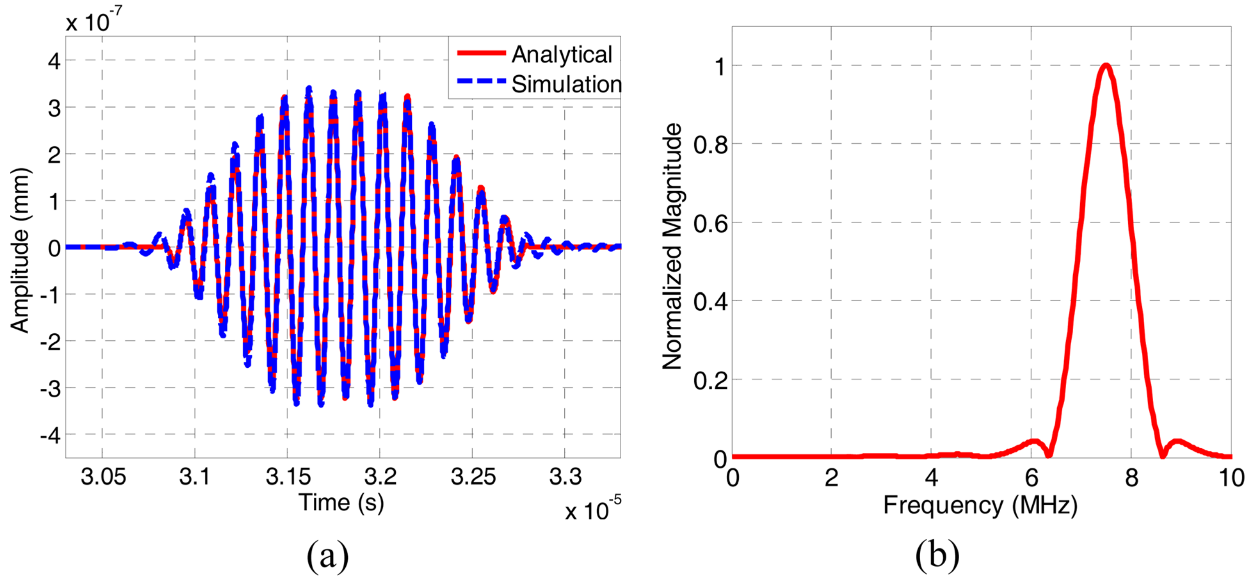

FIG. 4. (Color online) Waveform (a) and frequency spectrum (b) of the resonant wave generated by the two-way mixing of a longitudinal and a transverse pulse.

VI. COMPARISON WITH EXPERIMENTAL MEASUREMENTS

Ultrasonic measurement of two-way mixing of longitudinal and transverse pulses have been carried out on aluminum block samples[5] to investigate the resonant behavior, and on aluminum bar samples to detect plastic deformation.[6] In this paper, one-way mixing measurements are performed. The test setup is similar to that used in Refs. 5 and 6.

Briefly, a schematic of the experimental setup is shown in Fig. 5. Experimental measurements are conducted on an Al-6061 block of $75 \times 75 \times 150\,\text{mm}^3$. A high power gated amplifier RAM-5000 SNAP (RITEC Inc., Warwick, RI) is used as the pulse generator and the internal trigger signal from the RAM-5000 SNAP is used as a reference trigger. A dual-element transducer is used, which contains two D-shaped PZT elements. One of the elements generates a broadband transverse wave with a central frequency of 5 MHz, and the other generates a narrow-band longitudinal wave with a central frequency of 10 MHz. A RDX-6 diplexer (RITEC Inc., Warwick, RI) enables the transverse wave element to serve as both a transmitter and a receiver. The received resonant wave is digitized by a Tektronix TDS 5034B oscilloscope with a sampling frequency of 625 MHz and 10 000 sample points with 300 times average to increase the signal-to-noise ratio (SNR). The digitized time-domain signal is then sent to a computer for signal processing with Matlab.

In the experiment, the dual-element transducer is attached to one surface of the aluminum block. The transverse wave element emits a pulse consisting of 20 cycles of a sinusoidal wave with frequency 7.5 MHz, while the longitudinal wave element emits a pulse consisting of 10 cycles of a sinusoidal pulse of frequency 10 MHz. These two primary pulses mix at a desired location determined by the triggering timing of the two elements. The mixing generates a resonant wave propagating backward toward the transverse wave transducer. To isolate the resonant wave, time-domain signals of the two primary waves are subtracted from the total time-domain signal received by the transverse wave

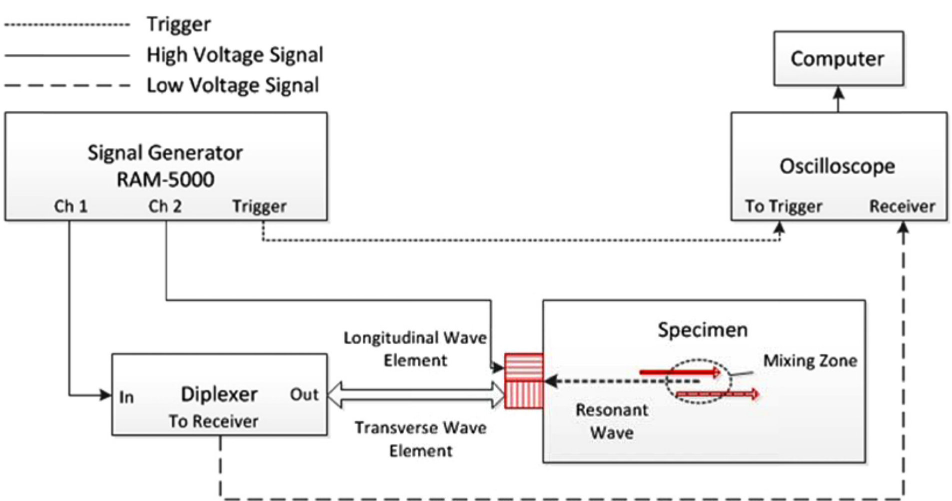

FIG. 5. (Color online) Schematic of collinear wave mixing experiment.

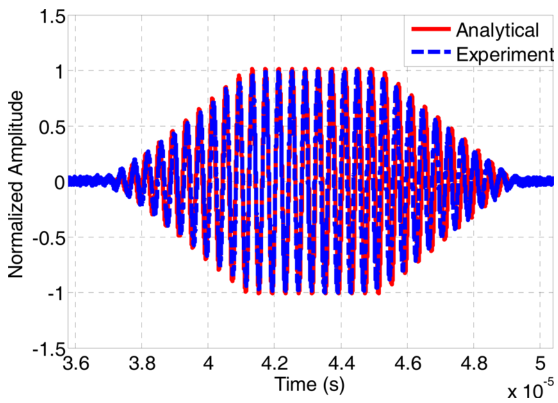

FIG. 6. (Color online) Waveform of the resonant wave generated by one-way mixing of a longitudinal pulse and transverse pulse. Solid line is from the analytical solution, and dashed line is from the experimental measurement.

receiver. The measured waveform of the resonant wave is shown in Fig. 6 as a dashed line. As discussed in Sec. IV, the waveform has a hexagonal shape, because $c_T\tau_T > c_L\tau_L$. The solid line in Fig. 6 is from the analytical solution derived in Sec. IV. Excellent agreement between the analytical solution and the experimental measurement is observed. This demonstrates that collinear one-way mixing could be a viable experimental technique to assess the acoustic nonlinearity parameter at a desired location inside a sample. We note that one-way mixing requires only one-sided access to the sample. This makes the one-way mixing technique valuable in many field NDE applications when access is available from only one side of the component to be tested.

VII. SUMMARY AND CONCLUSIONS

In this paper, we derived the necessary and sufficient conditions for generating resonant waves by two propagating time-harmonic plane waves. It was shown that in collinear mixing, a resonant wave can be generated either by a pair of longitudinal waves, in which case the resonant wave is a longitudinal wave, or by a pair of longitudinal and transverse waves, in which case the resonant wave is a transverse wave. In addition, we obtained closed-form analytical solutions to the resonant waves generated by two collinearly propagating sinusoidal pulses. We found that the waveform of the resonant wave has a hexagonal shape which reduces to a rhombus (diamond) shape when $c_L\tau_L = c_T\tau_T\ (\kappa+1)/2$ for one-way mixing or when $c_L\tau_L = c_T\tau_T\ (\kappa-1)/2$ for two-way mixing, where $c_L\tau_L$ and $c_T\tau_T$ are the spatial length of the longitudinal and transverse pulses, respectively. Further, amplitude of the resonant wave is proportional to $l_m = \min\{c_L\tau_L/(\kappa+1),\ c_T\tau_T/2\}$ for one-way mixing, and $l_m = \min\{c_T\tau_T/2,\ c_L\tau_L/(\kappa-1)\}$ for two-way mixing.

Furthermore, the paper investigated the feasibility of using the finite element method to simulate the mixing of two nonlinear waves. It was found that in order to capture the nonlinear interaction, there should be no less than 20 elements per wavelength of the highest frequencies in the problem. Finally, experimental measurements were conducted to demonstrate the feasibility of using one-way mixing as a nondestructive evaluation method. The results show excellent agreement between our experimental measurements and our predictions from the analytical solutions. This demonstrated that one-way mixing is a promising NDE technique for measuring the acoustic nonlinearity parameter at a desired location inside a bulk sample using access from only one side of the sample.

ACKNOWLEDGMENTS

This research is being performed using funding received from the DOE Office of Nuclear Energy's Nuclear Energy University Programs.

APPENDIX A

Consider

$$I(t) = \int_{-\infty}^{\infty}\int_{-\infty}^{\infty} \sin\left[\omega_R\left(\tau + \frac{s}{c_T}\right) + \phi_-\right] \times Q(s,\tau)\mathrm{H}\left(t - \tau - \frac{|s|}{c_T}\right) ds d\tau. \tag{A1}$$

To evaluate $I(t)$, we perform a transformation of variable, $s = c_T\hat{s}$. The integral can then be written as

$$I(t) = c_T\int_{-\infty}^{\infty}\int_{-\infty}^{\infty} \sin\left[\omega_R(\tau + \hat{s}) + \phi_-\right] \times Q(\hat{s},\tau)\mathrm{H}(t - \tau - |\hat{s}|) d\hat{s} d\tau. \tag{A2}$$

First, we note that

$$\begin{aligned} Q(\hat{s},\tau) &= P\left(\tau - t_L - \frac{\hat{s}}{\kappa}, \tau_L\right)P(\tau - t_T - \hat{s}, \tau_T) \\ &= \mathrm{H}\left(\tau - t_L - \frac{\hat{s}}{\kappa}\right)\mathrm{H}\left(\tau_L - \tau + t_L + \frac{\hat{s}}{\kappa}\right) \\ &\quad \times \mathrm{H}(\tau - t_T - \hat{s})\mathrm{H}(\tau_T - \tau + t_L + \hat{s}), \end{aligned} \tag{A3}$$

where $\kappa = c_L/c_T$ is defined in Sec. II. Obviously, $Q(s,\ \tau) = 1$ if and only if

$$\kappa(\tau - t_L - \tau_L) < \hat{s} < \kappa(\tau - t_L), \quad \tau - t_T - \tau_T < \hat{s} < \tau - t_T \tag{A4}$$

are both satisfied. Otherwise, $Q(\hat{s},\ \tau) = 0$. One may then define two pairs of parallel lines in the $\hat{s}$-τ plane,

$$\begin{aligned} \ell_L^u &= \{\hat{s}, \tau; \hat{s} = \kappa(\tau - t_L)\}, \\ \ell_L^d &= \{\hat{s}, \tau; \hat{s} = \kappa(\tau - t_L - \tau_L)\}, \end{aligned} \tag{A5}$$

$$\begin{aligned} \ell_T^u &= \{s, \tau; \hat{s} = \tau - t_T\}, \\ \ell_T^d &= \{\hat{s}, \tau; \hat{s} = \tau - t_T - \tau_T\}. \end{aligned} \tag{A6}$$

It is easy to show that (A4) defines a parallelogram $\square A_1A_2A_4A_3$ formed by these two pairs of parallel lines as shown by the shaded area in Fig. 7. For $c_L\tau_L < c_T\tau_T$, the coordinates of the four vertexes of the parallelogram are $A_i(\tau_i,\ \hat{s}_i)$,

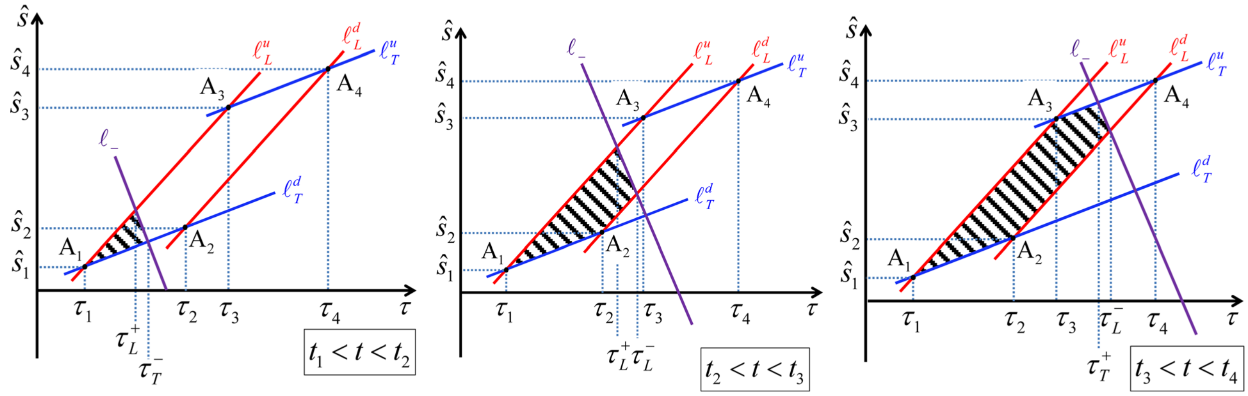

FIG. 7. (Color online) The shaded area is the domain on which the integrant of $I(t)$ is non-zero in the $\hat{s}$-τ plane during different time periods.

$$\tau_1 = \frac{c_L t_L - c_T(t_T + \tau_T)}{c_L - c_T}, \quad \hat{s}_1 = \frac{s_1}{c_T} = \frac{c_L(t_L - t_T - \tau_T)}{c_L - c_T}, \tag{A7}$$

$$\tau_2 = \frac{c_L(t_L + \tau_L) - c_T(t_T + \tau_T)}{c_L - c_T}, \quad \hat{s}_2 = \frac{s_2}{c_T} = \frac{c_L(t_L - t_T + \tau_L - \tau_T)}{c_L - c_T}, \tag{A8}$$

$$\tau_3 = \frac{c_L t_L - c_T t_T}{c_L - c_T}, \quad \hat{s}_3 = \frac{s_3}{c_T} = \frac{c_L(t_L - t_T)}{c_L - c_T}, \tag{A9}$$

$$\tau_4 = \frac{c_L(t_L + \tau_L) - c_T t_T}{c_L - c_T}, \quad \hat{s}_4 = \frac{s_4}{c_T} = \frac{c_L(t_L - t_T + \tau_L)}{c_L - c_T}. \tag{A10}$$

Next, consider $\mathrm{H}(t - \tau - |\hat{s}|)$. For it to be non-zero, one must have

$$t > \tau, \quad \tau - t < s < t - \tau. \tag{A11}$$

We define two lines by $\ell_- = \{\hat{s}, \tau; \hat{s} = -\tau + t\}$. It is easy to show that at $t = t_i$, the line ℓ_- intersects with the vertex $\hat{\mathrm{A}}_i$, where

$$t_1 = \frac{2c_L t_L - (c_L + c_T)(t_T + \tau_T)}{c_L - c_T}, \quad t_2 = t_1 + \frac{2c_L \tau_L}{c_L - c_T}, \tag{A12}$$

$$t_3 = t_1 + \frac{(c_L + c_T)\tau_T}{c_L - c_T}, \quad t_4 = t_3 + \frac{2c_L \tau_L}{c_L - c_T}. \tag{A13}$$

Clearly, to satisfy the second of Eq. (A11), a necessary condition is that s must be to the left of ℓ_-. Consequently, the non-zero domain for the integrant in Eq. (A1) is then the portion of the area of $\square \mathrm{A}_1\mathrm{A}_2\mathrm{A}_4\mathrm{A}_3$ that is to the left of ℓ_-, see the shaded area in Fig. 7. Therefore, the integral of Eq. (A1) can be viewed as an area integral

$$I(t) = c_T \int_{\Omega(t)} \sin[\omega_R(\tau + \hat{s}) + \phi_-] d\hat{s} d\tau, \tag{A14}$$

where $\Omega(t)$ is the shaded area as shown in Fig. 7 for the different time periods indicated on the figure. Obviously, for $t \le t_1$, no portion of $\square \mathrm{A}_1\mathrm{A}_2\mathrm{A}_4\mathrm{A}_3$ is to the left of ℓ_-. Thus, $I(t) = 0$ for $t \le t_1$. In what follows, we calculate $I(t)$ for $t > t_1$.

First, we introduce the gradient operator $\nabla \equiv [\partial/\partial\tau, \partial/\partial\hat{s}]$ and the Laplacian operator $\nabla^2 \equiv \partial^2/\partial\tau^2, \partial^2/\partial\hat{s}^2$. Then,

$$\nabla^2(\sin[\omega_R(\tau + \hat{s}) + \phi_-]) = -2\omega_R^2 \sin[\omega_R(\tau + \hat{s}) + \phi_-]. \tag{A15}$$

Making use of the Green's identity $\int_{\hat{\Omega}(t)} \nabla^2 \psi d s d\tau = \int_{\partial\hat{\Omega}(t)} \mathbf{n} \cdot \nabla\psi d s d\Gamma$, we arrive at

$$I(t) = -\frac{c_T}{2\omega_R} \int_{\partial\Omega(t)} [(1,1)\cdot\mathbf{n}] \cos[\omega_R(\tau + \hat{s}) + \phi_-] \times \sqrt{1 + \left(\frac{d\hat{s}}{d\tau}\right)^2} |d\tau|, \tag{A16}$$

where $\partial\Omega(t)$ is the boundary of $\Omega(t)$, $\mathbf{n}$ is the unit outward normal vector of $\partial\Omega(t)$, and the integration is counterclockwise along $\partial\Omega(t)$. Below, we will evaluate the contour integral along the different segments of the closed contour.

To this end, consider $\mathbf{n}$ along different segments of $\partial\hat{\Omega}(t)$,

$$\mathbf{n}|_{\ell_L^u} = -\mathbf{n}|_{\ell_L^d} = \frac{1}{\sqrt{1+\kappa^2}} \begin{bmatrix} -\kappa \\ 1 \end{bmatrix}, \quad \mathbf{n}|_{\ell_T^u} = -\mathbf{n}|_{\ell_T^d} = \frac{1}{\sqrt{2}} \begin{bmatrix} -1 \\ 1 \end{bmatrix}, \quad \mathbf{n}|_{\ell_-} = \frac{1}{\sqrt{2}} \begin{bmatrix} 1 \\ 1 \end{bmatrix}. \tag{A17}$$

Clearly, the integrand in Eq. (A16) vanishes along ℓ_T^u and ℓ_T^d because of $(1,1) \cdot \mathbf{n}|_{\ell_T^u} = (1,1) \cdot \mathbf{n}|_{\ell_T^d} = 0$. Thus $I(t)|_{\ell_T^u} = I(t)|_{\ell_T^d} = 0$. Along the other segments,

$$\begin{aligned} I_{\ell_L^u}(t,a,b) &\equiv I(t)|_{\ell_L^u} \\ &= \frac{c_T(\kappa - 1)}{2\omega_R} \int_a^b \cos[\omega_R(2\tau - t_L) + \phi_-] |d\tau| \\ &= \frac{c_T}{2\omega_T\omega_R} \sin[\omega_R(\kappa+1)\tau - t_L\omega_R\kappa + \phi_-]|_a^b, \end{aligned} \tag{A18}$$

$$\begin{aligned} I_{\ell_L^d}(t,a,b) &= I(t)|_{\ell_L^d} \\ &= -\frac{c_T(\kappa - 1)}{2\omega_R} \int_a^b \cos[\omega_R(2\tau - t_L - \tau_L) + \phi_-] |d\tau| \\ &= -\frac{c_T}{2\omega_R\omega_T} \sin[\omega_R(\kappa+1)\tau - (t_L + \tau_L)\omega_R\kappa + \phi_-]|_a^b, \end{aligned} \tag{A19}$$

$$I_{\ell_-}(t,a,b) = I(t)|_{\ell_-} = -\frac{c_T}{\omega_R}\int_a^b \cos[\omega_R t + \phi_-]|d\tau|$$
$$= -\frac{c_T}{\omega_R}(b-a)\cos[\omega_R t + \phi_-], \tag{A20}$$

where $b > a$ are the τ-coordinates of the two ends of the line segment.

Now, consider $t_1 < t < t_2$. In this range, the contour integral of Eq. (A16) consists of the following:

$$I(t) = I_{\ell_L^u}[t, \tau_L^+(t), \tau_1] + I_{\ell_-}[t, \tau_T^-(t), \tau_L^+(t)] \tag{A21}$$

where, and for future reference,

$$\tau_L^+(t) = \frac{c_T t + c_L t_L}{c_L + c_T}, \quad \tau_L^-(t) = \frac{c_T t + c_L(t_L + \tau_L)}{c_L + c_T}, \tag{A22}$$

$$\tau_T^+(t) = \frac{1}{2}(t + t_T), \quad \tau_T^-(t) = \frac{1}{2}(t + t_T + \tau_T) \tag{A23}$$

are the τ-coordinates of the intersections between ℓ_- and ℓ_L^u, ℓ_L^d, ℓ_T^u, and ℓ_T^d, respectively. Carrying out the integrals gives

$$I_{\ell_L^u}[t, \tau_1, \tau_L^+(t)] = \frac{c_T}{2\omega_T\omega_R}[\sin(\omega_R t + \phi_-) - \sin(\omega_R t_1 + \phi_-)], \tag{A24}$$

$$I_{\ell_-}[t, \tau_L^+(t), \tau_T^-(t)] = -\frac{c_T}{2\omega_T}(t - t_1)\cos(\omega_R t + \phi_-), \tag{A25}$$

where we have used the identifies

$$\frac{c_L + c_T}{c_L - c_T}\tau_T\omega_R = 2n_T\pi, \quad \frac{c_L\tau_L}{c_L - c_T}\omega_R = n_L\pi, \tag{A26}$$

with $n_{L,T}$ being integers.

For $t_2 < t < t_3$, the contour integral of Eq. (A16) consists of three line integrals,

$$I(t) = I_{\ell_L^u}[t, \tau_L^+(t), \tau_1] + I_{\ell_L^d}[t, \tau_2, \tau_L^-(t)] + I_{\ell_-}[t, \tau_L^-(t), \tau_L^+(t)]. \tag{A27}$$

Carrying out the integrals yields

$$I_{\ell_L^u}[t, \tau_L^+(t), \tau_1] + I_{\ell_L^d}[t, \tau_2, \tau_L^-(t)] = 0, \tag{A28}$$

$$I_{\ell_-}[t, \tau_L^+(t), \tau_L^-(t)] = -\frac{c_T}{2\omega_T}(t_2 - t_1)\cos(\omega_R t + \phi_-). \tag{A29}$$

For $t_3 < t < t_4$, the contour integral of Eq. (A16) consists of three line integrals,

$$I(t) = I_{\ell_L^u}[t, \tau_3, \tau_1] + I_{\ell_L^d}[t, \tau_2, \tau_L^-(t)] + I_{\ell_-}[t, \tau_L^-(t), \tau_T^+(t)]. \tag{A30}$$

Carrying them out yields

$$I_{\ell_L^u}[t, \tau_3, \tau_1] = 0, \tag{A31}$$

$$I_{\ell_L^d}[t, \tau_2, \tau_L^-(t)] = \frac{c_T}{2\omega_T\omega_R}[\sin(\omega_R t_4 + \phi_-) - \sin(\omega_R t + \phi_-)], \tag{A32}$$

$$I_{\ell_-}[t, \tau_L^-(t), \tau_T^+(t)] = -\frac{c_T}{2\omega_T}(t_4 - t)\cos(\omega_R t + \phi_-). \tag{A33}$$

Finally, for $t > t_4$, the integral is over the entire parallelogram $\square A_1A_2A_4A_3$. In this case, the contour integral of Eq. (A16) is the sum of integrals along $\overline{A_2A_4}$ and $\overline{A_1A_3}$, respectively, since the line integrals along $\overline{A_1A_2}$ and $\overline{A_3A_4}$ vanish. Thus,

$$I(t) = I_{\ell_L^u}[t, \tau_3, \tau_1] + I_{\ell_L^d}[t, \tau_2, \tau_4]. \tag{A34}$$

It can be easily shown that $I_{\ell_L^u}[t, \tau_3, \tau_1] = I_{\ell_L^d}[t, \tau_2, \tau_4] = 0$.

The above was derived for the case of $c_L\tau_L < c_T\tau_T$. It can be easily shown that the results are the same for $c_T\tau_T < c_L\tau_L < c_T\tau_T(\kappa+1)/2$. For $c_L\tau_L > c_T\tau_T(\kappa+1)/2$, the results are

$$I(t) = -\frac{c_T}{2\omega_T}(t - t_1)\cos(\omega_R t + \phi_-) + \frac{c_T}{2\omega_T\omega_R}[\sin(\omega_R t + \phi_-) - \sin(\omega_R t_1 + \phi_-)] \tag{A35}$$

for $t_1 < t < t_2$,

$$I(t) = -\frac{c_T}{2\omega_T}(t_2 - t_1)\cos(\omega_R t + \phi_-) + \frac{c_T}{2\omega_T\omega_R}[\sin(\omega_R t + \phi_-) - \sin(\omega_R t_3 + \phi_-)] \tag{A36}$$

for $t_2 < t < t_3$, and

$$I(t) = -\frac{c_T}{2\omega_T}(t_4 - t)\cos(\omega_R t + \phi_-) \tag{A37}$$

for $t_3 < t < t_4$. In the above,

$$t_1 = \frac{2c_L t_L - (c_L + c_T)(t_T + \tau_T)}{c_L - c_T}, \quad t_2 = t_1 + \frac{(c_L + c_T)\tau_T}{c_L - c_T}, \tag{A38}$$

$$t_3 = t_1 + \frac{2c_L\tau_L}{c_L - c_T}, \quad t_4 = t_3 + \frac{(c_L + c_T)\tau_T}{c_L - c_T}. \tag{A39}$$

Thus,

$$v(0,t) = \frac{\beta_T UV\omega_T^2}{2c_T^2(\kappa+1)}\left(\frac{c_T\tau_T}{2}\right)h(t, n_T), \tag{A40}$$

where

$$h(t,n_T)=\begin{cases}\dfrac{t-t_1}{t_2-t_1}\cos(\omega_R t+\phi_-)-\dfrac{1}{2n_T\pi}[\sin(\omega_R t+\phi_-)-\sin(\omega_R t_1+\phi_-)] & \text{for } t_1<t<t_2\\ \cos(\omega_R t+\phi_-)-\dfrac{1}{2n_T\pi}[\sin(\omega_R t+\phi_-)-\sin(\omega_R t_3+\phi_-)] & \text{for } t_2<t<t_3\\ \dfrac{t_4-t}{t_4-t_3}\cos(\omega_R t+\phi_-) & \text{for } t_3<t<t_4.\end{cases} \tag{A41}$$

APPENDIX B

We need to evaluate

$$I(t)=c_T\int_{-\infty}^{\infty}\int_{-\infty}^{\infty}\sin[\omega_R(\tau+\hat{s})-\phi_-]Q(\hat{s},\tau)\mathrm{H}(t-\tau-|\hat{s}|)d\hat{s}d\tau. \tag{B1}$$

Note that

$$Q(\hat{s},\tau)=P\left(\tau-t_L-\frac{\hat{L}-\hat{s}}{\kappa},\tau_L\right)P(\tau-t_T-\hat{s},\tau_T)=\mathrm{H}\left(\tau-t_L-\frac{\hat{L}-\hat{s}}{\kappa}\right)\mathrm{H}\left(\tau_L-\tau+t_L+\frac{\hat{L}-\hat{s}}{\kappa}\right)$$
$$\times\,\mathrm{H}(\tau-t_T-\hat{s})\mathrm{H}(\tau_T-\tau+t_T+\hat{s}), \tag{B2}$$

where $\hat{L}=L/c_T$ is introduced in Sec. IV. Obviously, $Q(\hat{s},\tau)=1$ if and only if

$$\hat{L}-\kappa(\tau-t_L)<\hat{s}<\hat{L}-\kappa(\tau-t_L-\tau_L),\quad \tau-t_T-\tau_T<\hat{s}<\tau-t_T \tag{B3}$$

are both satisfied. Otherwise, $Q(\hat{s},\tau)=0$. One may then define two pairs of parallel lines in the $\hat{s}$-τ plane,

$$\ell_L^u=\{\hat{s},\tau;\hat{s}=\hat{L}-\kappa(\tau-t_L)\},\quad \ell_L^d=\{\hat{s},\tau;\hat{s}=\hat{L}-\kappa(\tau-t_L-\tau_L)\}, \tag{B4}$$

$$\ell_T^u=\{s,\tau;\hat{s}=\tau-t_T\},\quad \ell_T^d=\{\hat{s},\tau;\hat{s}=\tau-t_T-\tau_T\}. \tag{B5}$$

It is easy to show that Eq. (B3) defines a parallelogram $\varDelta A_1A_3A_4A_2$, see Fig. 8. The coordinates of the four vertexes of the parallelogram are, respectively, $A_1(\tau_3,s_1)$, $A_2(\tau_1,s_3)$, $A_3(\tau_4,s_2)$, and $A_4(\tau_2,s_4)$, where

$$\tau_1=\frac{L+c_Lt_L+c_Tt_T}{c_L+c_T},\quad \tau_2=\frac{L+c_L(t_L+\tau_L)+c_Tt_T}{c_L+c_T}, \tag{B6}$$

$$\tau_3=\frac{L+c_Lt_L+c_T(t_T+\tau_T)}{c_L+c_T},\quad \tau_4=\frac{L+c_L(t_L+\tau_L)+c_T(t_T+\tau_T)}{c_L+c_T}, \tag{B7}$$

$$\hat{s}_1=\frac{s_1}{c_T}=\frac{L+c_L(t_L-t_T-\tau_T)}{c_L+c_T},\quad \hat{s}_2=\frac{s_2}{c_T}=\frac{L+c_L(t_L-t_T+\tau_L-\tau_T)}{c_L+c_T}, \tag{B8}$$

$$\hat{s}_3=\frac{s_3}{c_T}=\frac{L+c_L(t_L-t_T)}{c_L+c_T},\quad \hat{s}_4=\frac{s_4}{c_T}=\frac{L+c_L(t_L-t_T+\tau_L)}{c_L+c_T}. \tag{B9}$$

Next, consider $\mathrm{H}(t-\tau-|\hat{s}|)$. For it to be non-zero, one must have

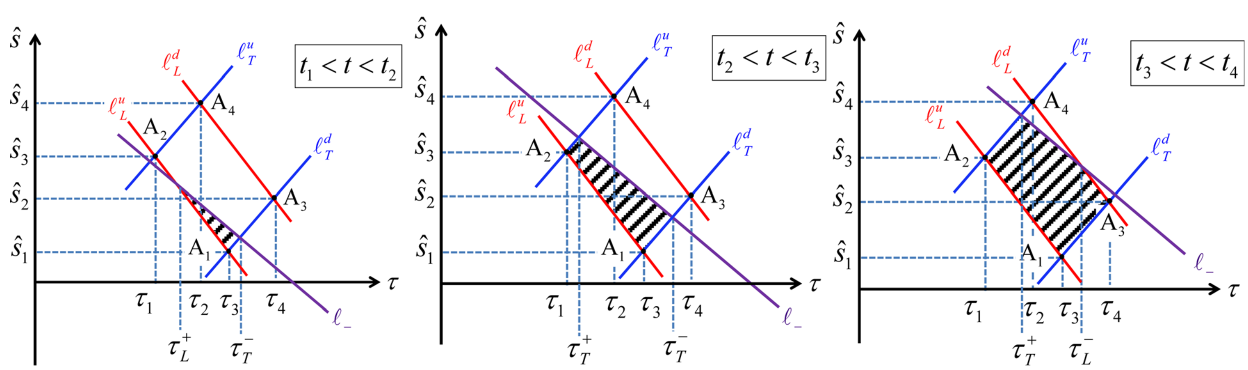

FIG. 8. (Color online) Shaded area is the domain over which the integrant of $I(t)$ is non-zero the $\hat{s}$-τ plane for different periods of time.

$$t > \tau, \quad \tau - t < s < t - \tau. \tag{B10}$$

We define a line by $\ell_- = \{\hat{s}, \tau; \hat{s} = -\tau + t\}$. It is easy to show that at $t = t_i$, the line ℓ_- intersects with the vertex A_i, where

$$t_1 = \frac{2(L + c_L t_L) - (c_L - c_T)(t_T + \tau_T)}{c_L + c_T},$$
$$t_2 = t_1 + \frac{(c_L - c_T)\tau_T}{c_L + c_T}, \tag{B11}$$

$$t_3 = t_1 + \frac{2c_L\tau_L}{c_L + c_T}, \quad t_4 = t_2 + \frac{2c_L\tau_L}{c_L + c_T}. \tag{B12}$$

Clearly, to satisfy the second equation of Eq. (B10), a necessary condition is that $\hat{s}$ must be to the left of ℓ_-. Consequently, the non-zero domain for the integral in Eq. (B1) is then the portion of the area of $\square A_1A_3A_4A_2$ that is to the left of ℓ_-, see the shaded area in Fig. 8. Therefore, the integral of Eq. (B1) can be viewed as an area integral,

$$I(t) = c_T \int_{\Omega(t)} \sin[\omega_R(\tau + \hat{s}) - \phi_-] d\hat{s} d\tau, \tag{B13}$$

where $\Omega(t)$ is the shaded area shown in Fig. 8 during different periods of time.

Following the approach used in Appendix A, we can convert the area integral of Eq. (B13) into a contour integral,

$$I(t) = -\frac{c_T}{2\omega_R} \int_{\partial\Omega(t)} [(1,1)\cdot\mathbf{n}] \cos[\omega_R(\tau + \hat{s}) - \phi_-] \times \sqrt{1 + \left(\frac{d\hat{s}}{d\tau}\right)^2} |d\tau|, \tag{B14}$$

where $\partial\Omega(t)$ is the boundary of $\Omega(t)$, and $\mathbf{n}$ is the unit outward normal vector of $\partial\Omega(t)$. Obviously, for $t \le t_1$, no portion of $\square A_1A_3A_4A_2$ is to the left of ℓ_-. Thus, $I(t) = 0$ for $t \le t_1$. In what follows, we calculate $I(t)$ for $t > t_1$.

To this end, consider $\mathbf{n}$ along different segments of $\partial\hat{\Omega}(t)$,

$$\mathbf{n}|_{\ell_L^u} = -\mathbf{n}|_{\ell_L^d} = \frac{-1}{\sqrt{1+\kappa^2}} \begin{bmatrix} \kappa \\ 1 \end{bmatrix},$$
$$\mathbf{n}|_{\ell_T^u} = -\mathbf{n}|_{\ell_T^d} = \frac{1}{\sqrt{2}} \begin{bmatrix} -1 \\ 1 \end{bmatrix}, \quad \mathbf{n}|_{\ell_-} = \frac{1}{\sqrt{2}} \begin{bmatrix} 1 \\ 1 \end{bmatrix}. \tag{B15}$$

Clearly, the integrand in Eq. (B14) vanishes along ℓ_T^u and ℓ_T^d because of $(1,1)\cdot\mathbf{n}|_{\ell_T^u} = (1,1)\cdot\mathbf{n}|_{\ell_T^d} = 0$. Thus $I(t)|_{\ell_T^u} = I(t)|_{\ell_T^d} = 0$. Along the other segments,

$$I_{\ell_L^u}(t,a,b) \equiv I(t)|_{\ell_L^u} = \frac{c_T(\kappa+1)}{2\omega_R} \int_a^b \cos\{\omega_R[(L - \tau(\kappa-1) + \kappa t_L) - \phi_-]\} |d\tau|$$
$$= \frac{c_T}{2\omega_R\omega_T} \sin[-(\kappa-1)\tau\omega_R + (L + \kappa t_L)\omega_R - \phi_-]|_a^b, \tag{B16}$$

$$I_{\ell_L^d}(t,a,b) = I(t)|_{\ell_L^d} = -\frac{c_T(\kappa+1)}{2\omega_R} \int_a^b \cos\{\omega_R[L - \tau(\kappa-1) + \kappa(t_L + \tau_L)] - \phi_-\} |d\tau|$$
$$= -\frac{c_T}{2\omega_R\omega_T} \sin[-(\kappa-1)\tau\omega_R + (L + \kappa t_L + \kappa\tau_L)\omega_R - \phi_-]|_a^b, \tag{B17}$$

$$I_{\ell_-}(t,a,b) = I(t)|_{\ell_-} = -\frac{c_T}{\omega_R} \int_a^b \cos[\omega_R t - \phi_-] |d\tau|$$
$$= -\frac{c_T}{\omega_R}(b-a)\cos[\omega_R t - \phi_-], \tag{B18}$$

where $a < b$ are the τ-coordinates of the two ends of the line segment.

Next, consider $t_1 < t < t_2$. In this range, the contour integral of Eq. (B14) consists of the following:

$$I(t) = I_{\ell_L^u}[t, \tau_L^+(t), \tau_1] + I_{\ell_-}[t, \tau_L^-(t), \tau_L^+(t)], \tag{B19}$$

where, and for future reference,

$$\tau_L^+(t) = \frac{L - c_T t + c_L t_L}{c_L - c_T}, \quad \tau_L^-(t) = \frac{L - c_T t + c_L(t_L + \tau_L)}{c_L - c_T}, \tag{B20}$$

$$\tau_T^+(t) = \frac{1}{2}(t + t_T), \quad \tau_T^-(t) = \frac{1}{2}(t + t_T + \tau_T) \tag{B21}$$

are the τ-coordinates of the intersections between ℓ_- and ℓ_L^u, ℓ_L^d, ℓ_T^u, and ℓ_T^d, respectively. Carrying out the integrals gives

$$I_{\ell_L^u}[t, \tau_1, \tau_L^+(t)] = \frac{c_T}{2\omega_T\omega_R}[\sin(\omega_R t - \phi_-) - \sin(\omega_R t_1 - \phi_-)], \tag{B22}$$

$$I_{\ell_-}[t, \tau_L^+(t), \tau_T^-(t)] = -\frac{c_T}{2\omega_T}(t - t_1)\cos(\omega_R t - \phi_-), \tag{B23}$$

where we have used the identities,

$$\frac{c_L - c_T}{c_L + c_T}\tau_T\omega_R = 2n_T\pi, \quad \frac{c_L\tau_L}{c_L + c_T}\omega_R = n_L\pi, \tag{B24}$$

with $n_{L,T}$ being integers.

For $t_2 < t < t_3$, the contour integral of Eq. (B14) consists of two line integrals,

$$I(t) = I_{\ell_L^u}[t, \tau_2, \tau_1] + I_{\ell_-}[t, \tau_T^-(t), \tau_T^+(t)]. \quad \text{(B25)}$$

Carrying out the integrals yields

$$\begin{aligned} &I_{\ell_L^u}[t, \tau_2, \tau_1] = 0, \\ &I_{\ell_-}\left[t, \tau_L^-(t), \tau_L^+(t)\right] = -\frac{c_T}{2\omega_T}(t_2 - t_1)\cos(\omega_R t - \phi_-). \end{aligned} \quad \text{(B26)}$$

For $t_3 < t < t_4$, the contour integral of Eq. (B14) consists of two line integrals,

$$I(t) = I_{\ell_L^u}[t, \tau_2, \tau_1] + I_{\ell_-}[t, \tau_3, \tau_L^-(t),] + I_{\ell_L^d}[t, \tau_L^-(t), \tau_T^+(t)]. \quad \text{(B27)}$$

Carrying them out yields

$$\begin{aligned} &I_{\ell_L^u}[t, \tau_2, \tau_1] = 0, \\ &I_{\ell_-}\left[t, \tau_T^+(t), \tau_L^-(t)\right] = -\frac{c_T}{2\omega_T}(t_4 - t)\cos(\omega_R t - \phi_-) \end{aligned} \quad \text{(B28)}$$

$$I_{\ell_L^d}\left[t, \tau_3, \tau_L^-(t)\right] = \frac{c_T}{2\omega_T\omega_R}[\sin(\omega_R t_4 - \phi_-) - \sin(\omega_R t - \phi_-)].$$

Finally, for $t > t_4$, the integral is over the entire parallelogram $\square A_1A_3A_4A_2$. In this case, the contour integral of Eq. (B14) is the sum of integrals along $\overline{A_1A_2}$ and $\overline{A_3A_4}$, respectively, since the line integrals along $\overline{A_2A_4}$ and $\overline{A_1A_3}$ both vanish. Thus,

$$I(t) = I_{\ell_L^u}[t, \tau_2, \tau_1] + I_{\ell_L^d}[t, \tau_3, \tau_4]. \quad \text{(B29)}$$

It is easy to show that $I_{\ell_L^u}(t, \tau_2, \tau_1) = I_{\ell_L^d}(t, \tau_3, \tau_4) = 0$.

The above results are for $c_T\tau_T(\kappa - 1)/2 < c_L\tau_L < c_T\tau_T$. It can be shown that for $c_L\tau_L > c_T\tau_T$, the results are the same. For the case of $c_L\tau_L < c_T\tau_T(\kappa - 1)/2$, the results are

$$\begin{aligned} I(t) = &-\frac{c_T}{2\omega_T}(t - t_1)\cos(\omega_R t - \phi_-) \\ &+ \frac{c_T}{2\omega_T\omega_R}[\sin(\omega_R t - \phi_-) - \sin(\omega_R t_1 - \phi_-)] \end{aligned} \quad \text{(B30)}$$

for $t_1 < t < t_2$,

$$I(t) = -\frac{c_T}{2\omega_T}(t_2 - t_1)\cos(\omega_R t - \phi_-) \quad \text{(B31)}$$

for $t_2 < t < t_3$, and

$$\begin{aligned} I(t) = &-\frac{c_T}{2\omega_T}(t_4 - t)\cos(\omega_R t - \phi_-) + \frac{c_T}{2\omega_T\omega_R} \\ &\times [\sin(\omega_R t_4 - \phi_-) - \sin(\omega_R t - \phi_-)] \end{aligned} \quad \text{(B32)}$$

for $t_3 < t < t_4$, where

$$\begin{aligned} t_1 &= \frac{2(L + c_L t_L) - (c_L - c_T)(t_T + \tau_T)}{c_L + c_T}, \\ t_2 &= t_1 + \frac{2c_L\tau_L}{c_L + c_T} \end{aligned} \quad \text{(B33)}$$

$$t_3 = t_1 + \frac{(c_L - c_T)\tau_T}{c_L + c_T}, \quad t_4 = t_2 + \frac{(c_L - c_T)\tau_T}{c_L + c_T}. \quad \text{(B34)}$$

Consequently,

$$v(0, t) = \frac{\beta_T U V \omega_T^2}{2c_T^2(\kappa - 1)}\left(\frac{c_L\tau_L}{\kappa - 1}\right)g(t, n_L, -\phi_-), \quad \text{(B35)}$$

where $g(t,\ n_L,\ -\phi_-)$ is defined in Eq. (55) with the understanding that the t_i used in $g(t,\ n_L,\ -\phi_-)$ are those listed in Eqs. (B33) and (B34).

[1] G. L. Jones and D. R. Kobett, "Interaction of elastic waves in an isotropic solid," J. Acoust. Soc. Am. **35**, 5 (1963).

[2] F. R. Rollins, "Interaction of ultrasonic waves in solid media," Appl. Phys. Lett. **2**(8), 147–148 (1963).

[3] P. A. Johnson, T. J. Shankland, R. J. O'Connell, and J. N. Albright, "Nonlinear generation of elastic waves in crystalline rock," J. Geophys. Res.: Solid Earth **92**(B5), 3597–3602, doi:10.1029/JB092iB05p03597 (1987).

[4] V. A. Korneev and A. Demcenko, "Possible second-order nonlinear interactions of plane waves in an elastic solid," J. Acoust. Soc. Am. **135**(2), 591–598 (2014).

[5] M. H. Liu, G. X. Tang, L. J. Jacobs, and J. Qu, "Measuring acoustic nonlinearity parameter using collinear wave mixing," J. Appl. Phys. **112**(2) 024908 (2012).

[6] G. Tang, M. Liu, L. J. Jacobs, and J. Qu, "Detecting localized plastic strain by a scanning collinear wave mixing method," J. Nondestr. Eval. **33**, 196–204 (2014).

[7] J. P. Jiao, J. J. Sun, N. Li, G. R. Song, B. Wu, and C. F. "He, Micro-crack detection using a collinear wave mixing technique," NDT & E Int. **62**, 122–129 (2014).

[8] A. Demcenko, R. Akkerman, P. B. Nagy, and R. Loendersloot, "Non-collinear wave mixing for non-linear ultrasonic detection of physical ageing in pvc," NDT & E Int. **49**, 34–39 (2012).

[9] A. J. Croxford, P. D. Wilcox, B. W. Drinkwater, and P. B. Nagy, "The use of non-collinear mixing for nonlinear ultrasonic detection of plasticity and fatigue," J. Acoust. Soc. Am. **126**(5), EL117–EL122 (2009).

[10] E. Escobar-Ruiz, A. Ruiz, W. Hassan, D. C. Wright, I. J. Collison, P. Cawley, and P. B. Nagy, "Non-linear ultrasonic NDE of titanium diffusion bonds," J. Nondestr. Eval. **33**(2), 187–195 (2014).

[11] A. Demcenko, V. Koissin, and V. A. Korneev, "Noncollinear wave mixing for measurement of dynamic processes in polymers: Physical ageing in thermoplastics and epoxy cure," Ultrasonics **54**(2), 684–693 (2014).

[12] G. X. Tang, L. J. Jacobs, and J. Qu, "Scattering of time-harmonic elastic waves by an elastic inclusion with quadratic nonlinearity," J. Acoust. Soc. Am. **131**(4), 2570–2578 (2012).

[13] M. Dubuget, R. E. Guerjouma, S. Dubois, J. C. Baboux, and A. Vincent, "Characterization of the non-linear elastic properties of aluminium alloys using ultrasonic evaluation under load," Mater. Sci. Forum **217–222**, 951–956 (1996).

[14] C. Valle, M. Niethammer, J. Qu, and L. J. Jacobs, "Crack characterization using guided circumferential waves," J. Acoust. Soc. Am. **110**(3), 1282–1290 (2001).

[15] C. Valle, J. Qu, and L. J. Jacobs, "Guided circumferential waves in layered cylinders," Int. J. Eng. Sci. **37**(11), 1369–1387 (1999).